Neuron
Article

# Feedback Inhibition Enables Theta-Nested Gamma Oscillations and Grid Firing Fields

Hugh Pastoll,[1,2,3] Lukas Solanka,[2,3] Mark C.W. van Rossum,[2] and Matthew F. Nolan[1,*]
[1]Centre for Integrative Physiology, University of Edinburgh, Hugh Robson Building, Edinburgh EH8 9XD, UK
[2]Institute for Adaptive and Neural Computation
[3]Neuroinformatics Doctoral Training Centre
School of Informatics, University of Edinburgh, Edinburgh EH8 9AB, UK
*Correspondence: mattnolan@ed.ac.uk
http://dx.doi.org/10.1016/j.neuron.2012.11.032

## SUMMARY

**Cortical circuits are thought to multiplex firing rate codes with temporal codes that rely on oscillatory network activity, but the circuit mechanisms that combine these coding schemes are unclear. We establish with optogenetic activation of layer II of the medial entorhinal cortex that theta frequency drive to this circuit is sufficient to generate nested gamma frequency oscillations in synaptic activity. These nested gamma oscillations closely resemble activity during spatial exploration, are generated by local feedback inhibition without recurrent excitation, and have clock-like features suitable as reference signals for multiplexing temporal codes within rate-coded grid firing fields. In network models deduced from our data, feedback inhibition supports coexistence of theta-nested gamma oscillations with attractor states that generate grid firing fields. These results indicate that grid cells communicate primarily via inhibitory interneurons. This circuit mechanism enables multiplexing of oscillation-based temporal codes with rate-coded attractor states.**

## INTRODUCTION

Cortical neurons encode information through the rate and timing of their action potential output (Buzsáki and Draguhn, 2004; Fries, 2009; Huxter et al., 2003; O'Keefe and Recce, 1993). At the same time, activity in networks of cortical neurons oscillates with frequency and amplitude that depend on behavioral state (Buzsáki, 2002; Buzsáki and Draguhn, 2004; Buzsáki and Wang, 2012; Canolty and Knight, 2010; Fries, 2009; Klausberger and Somogyi, 2008). Cortical network oscillations are believed to be critical for temporal codes (Buzsáki and Draguhn, 2004; Buzsáki and Wang, 2012; Colgin et al., 2009; Fries, 2009; Lisman, 2005) and coupling between oscillatory activity in different frequency bands appears to be a general feature of cognitive states (Buzsáki and Draguhn, 2004; Buzsáki and Wang, 2012; Canolty and Knight, 2010). However, the cellular mechanisms that coordinate interactions between oscillations in different frequency bands are not known. The relationships between mechanisms that generate oscillatory reference signals and those that support representation of information through firing rate codes are also not clear.

Grid cells in layer II of the medial entorhinal cortex (MEC) represent location relative to the external environment using rate-coded grid-like firing fields and by timing of their action potentials relative to theta frequency (4–12 Hz) network rhythms (Fyhn et al., 2004; Hafting et al., 2005, 2008). Nested within the slower theta rhythm are network oscillations with frequency in the high gamma range (60–120 Hz) (Chrobak and Buzsáki, 1998; Colgin et al., 2009). These gamma frequency oscillations are believed to act as a reference signal to coordinate interactions between MEC neurons and their synaptic partners in the hippocampus (Buzsáki and Draguhn, 2004; Colgin et al., 2009), so that ensembles of MEC neurons with firing that is phase locked to nested gamma oscillations more effectively activate downstream neurons on which their synaptic output converges (Buzsáki and Wang, 2012; Fries, 2009). Nested gamma oscillations are also hypothesized to enable temporal codes in which different items are encoded on each gamma cycle (Lisman, 2005). However, the cellular mechanisms that enable generation of grid firing fields and theta-nested gamma oscillations are not clear. The possibility that theta frequency drive is sufficient for generation of nested gamma oscillations has not previously been addressed. It is also not clear if the same circuit mechanisms generate nested oscillatory activity and grid firing fields, or if instead either form of activity requires additional circuit elements.

Because encoding of location by grid cells in layer II of the MEC requires inputs from the medial septum and as activity of these inputs is modulated at theta frequency (Brandon et al., 2011; Koenig et al., 2011; Mitchell et al., 1982), we set out to investigate whether theta frequency activation of layer II networks is sufficient to generate nested gamma oscillations. Using optogenetic stimulation, we demonstrate that theta frequency optical activation elicits nested gamma frequency oscillations that closely resemble activity observed during spatial behaviors. In contrast to pharmacologically induced gamma activity, optical nested oscillations have frequency in the high gamma band and

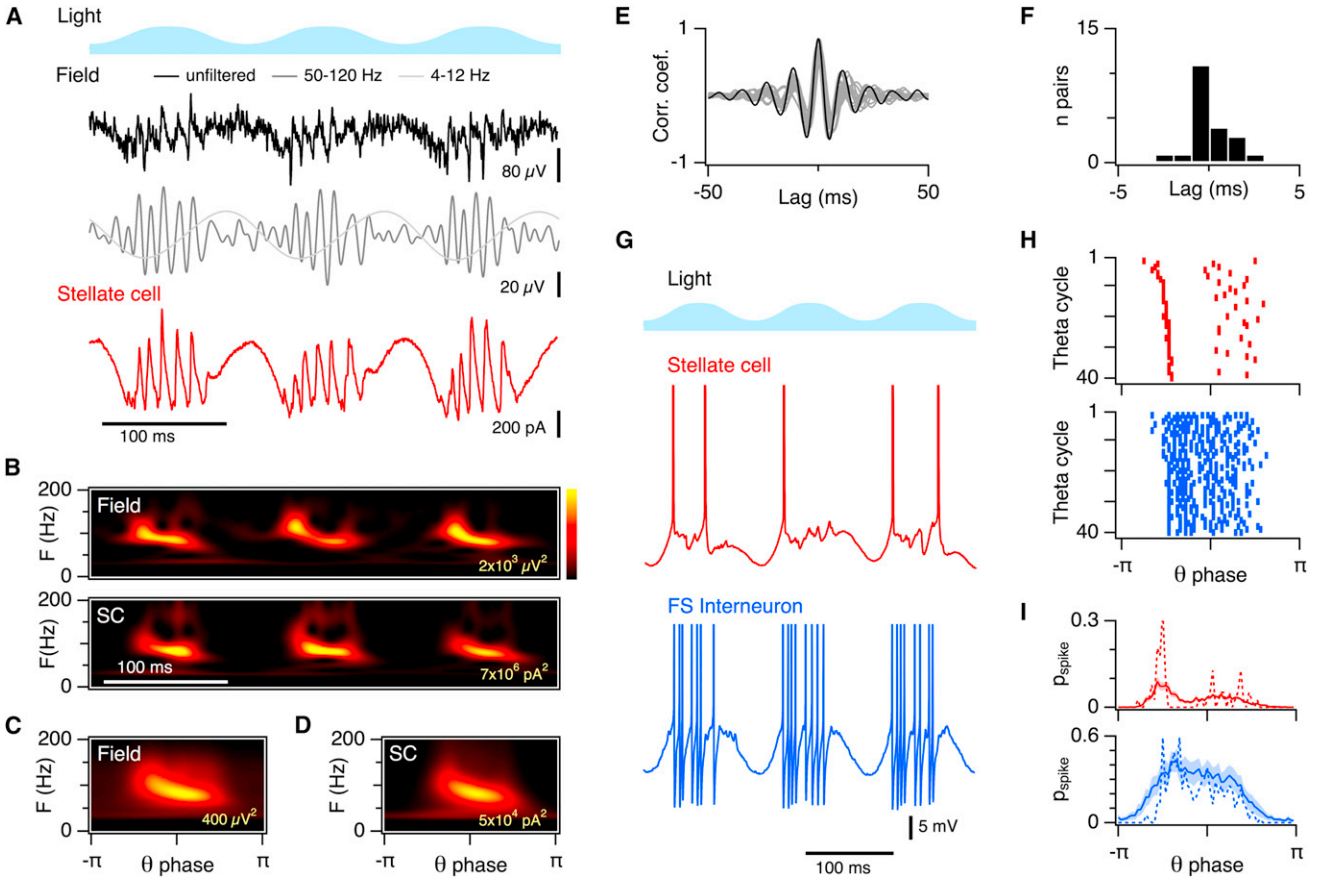


**Figure 1. Theta Frequency Stimulation Drives Nested Gamma Oscillations**

(A) Example of extracellular field activity and membrane current recorded from an SC during theta-modulated (8 Hz) optical stimulation of layer II of the MEC, illustrating gamma oscillations nested within each theta cycle. The field recording is also shown band-pass filtered to separate theta and gamma activity.

(B) Scalograms of field (top) and synaptic (bottom) activity corresponding to data in (A), plotting power for each frequency as a function of time. In all figures, the power corresponding to the maximum of the color scale is indicated in the bottom right of each plot.

(C and D) Mean scalograms from all recordings of field (C) (n = 27) and SC synaptic activity (D) (n = 44) as a function of phase of theta stimulation.

(E) Cross-correlations between field potential and SC membrane currents (peak correlation = 0.81 ± 0.02, lag 0.12 ± 0.2 ms, n = 21). Example from (A and B) is shown in black, all other experiments are shown in gray.

(F) Histogram of lag between field and SC synaptic activity calculated from (E).

(G) Examples of action potentials fired by an SC and an FS interneuron recorded simultaneously during 8 Hz light stimulation, illustrating that both neuron types fire action potentials on the phase of the theta cycle at which nested gamma oscillations are observed.

(H) Rasters of spikes fired by neurons in (G) for 40 consecutive theta epochs.

(I) Probability of SC and FS interneuron action potentials with respect to the phase of theta stimulation. Solid lines represent the population means, dashed lines represent the examples from (G). Shaded regions indicate SEM.

have clock-like properties that make them suitable for multiplexing temporal codes within rate-coded firing fields. Optical theta-nested gamma and pharmacologically induced gamma activity also differ in their underlying mechanism. Layer II of the MEC contains inhibitory interneurons and excitatory stellate cells (SCs) that are likely to correspond to grid cells (Burgalossi et al., 2011; Canto et al., 2008; Pastoll et al., 2012a), but the synaptic and functional interactions of SCs and interneurons have not been determined. We establish that nested gamma oscillations require synaptic interactions mediated by local feedback inhibition between SCs but do not involve recurrent excitation. Finally, we demonstrate that networks of excitatory neurons connected only by feedback inhibition are sufficient to generate grid firing fields through network attractor states and to simultaneously produce clock-like theta-nested gamma oscillations.

## RESULTS

### Local Theta Frequency Stimulation Is Sufficient to Generate Nested Gamma Frequency Network Oscillations

To test the sufficiency of local theta frequency activity in the MEC for generation of nested gamma frequency oscillations, we adopted an optogenetic approach (Figure 1 and see Figure S1 available online). We recorded activity from neurons in layer II of the MEC in brain slices prepared from adult mice.

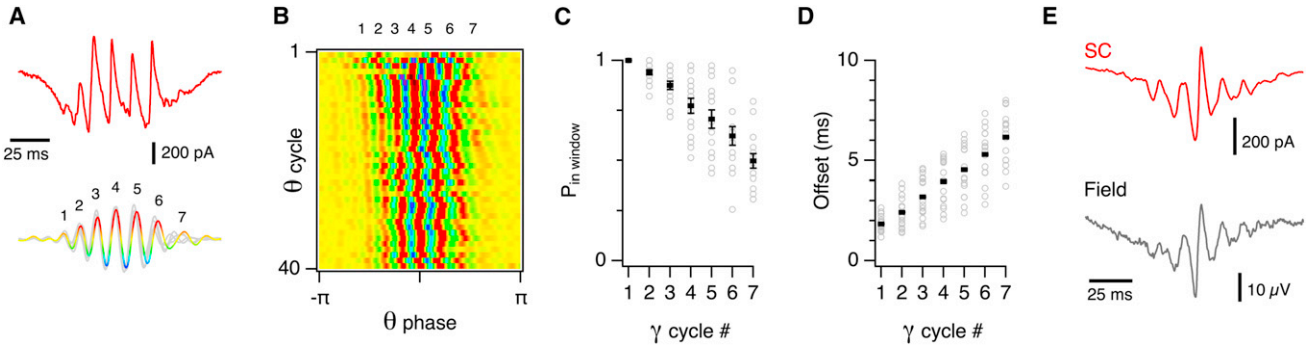


**Figure 2. Clock-like Properties of Nested Gamma Activity**

(A) Example of a membrane current recorded from an SC during a theta cycle (top) and corresponding filtered current (bottom, colored line). Also shown are filtered traces from four adjacent theta epochs (gray traces), illustrating the consistency of the nested gamma response between theta cycles.

(B) Heat map of membrane currents during 40 consecutive cycles of theta stimulation from the cell in (A). Color scale corresponds to (A).

(C and D) Fraction of gamma cycles on which the peak current differs by less than ± 5 ms (C), and average offset of individual gamma cycles compared to the mean (D) are plotted as a function of the index of each nested gamma peak. Open circles correspond to individual neurons and filled bars indicate the mean ± SEM (n = 12).

(E) Examples of traces obtained by averaging responses triggered from the trough of each gamma cycle recorded simultaneously from an SC (top) and the nearby field (bottom). The side peaks are consistent with periodic gamma activity.

We used a mouse line in which expression of channelrhodopsin-2 (ChR2) is under the control of the Thy1 promoter (Arenkiel et al., 2007). In this mouse line, all tested SCs and fast-spiking (FS) interneurons were depolarized by light, but pyramidal cells were not (Figure S1). We found that theta frequency (8 Hz) optical stimulation causes local field potential oscillations nested within each theta cycle (Figures 1A–1C). This nested activity had frequency 86.1 ± 2.4 Hz (range 62.4–100.8 Hz, n = 13), similar to the frequency of nested gamma activity reported in the MEC of behaving animals (Chrobak and Buzsáki, 1998; Colgin et al., 2009) and much higher than the frequency of pharmacologically induced gamma oscillations (Cunningham et al., 2003; Dickson et al., 2000; Middleton et al., 2008; van Der Linden et al., 1999).

To begin to investigate the synaptic mechanisms mediating nested gamma activity, we recorded membrane currents from SCs. We observed nested synaptic currents with frequency 82.7 ± 2.05 Hz (range 64.2–100.8, n = 21) (Figures 1A, 1B, and 1D). Cross-correlation analysis indicated that the timing of the nested synaptic currents was similar to simultaneously recorded theta-nested epochs of field gamma activity (peak correlation = 0.81 ± 0.02, lag 0.12 ± 0.2 ms, n = 21) (Figures 1E and 1F), indicating that they reflect the same process. Consistent with this conclusion, the frequency with maximum power for synaptic and simultaneously recorded field gamma activity was also highly correlated (slope = 0.94, $R^2 = 0.9$, $p = 4.2 \times 10^{-11}$, n = 21).

The nested synaptic currents recorded from SCs were outward going, suggesting that nested gamma oscillations involve inhibitory synaptic input to SCs (Figure 1A). We therefore recorded the membrane potential of SCs and nearby FS interneurons during theta stimulation (Figure 1G). SCs fired on average 1.5 ± 0.2 action potentials per theta epoch (n = 55), whereas interneurons fired 13.4 ± 3.1 spikes per epoch (n = 11) (Figure S1). Theta stimulation modulated the timing of action potential firing by both neuron types (44/48 SCs and 11/11 interneurons, $p < 0.05$ versus a uniform distribution, Kuiper test). Within each theta cycle, action potential firing by SCs and interneurons coincided with nested gamma oscillations (Figures 1G–1I) and the range of theta phases during which interneurons and SCs fired action potentials was similar (mean theta phase of first spike: SC −1.24 rads [from peak], n = 48, FS interneuron −1.72 rads, n = 11, p = 0.79, nonparametric second-order analysis of angles [NSOA]; mean theta phase of last spike: SC 0.96 rads, n = 37, FS interneuron 1.12 rads, n = 11, p = 0.37, NSOA). However, the distribution of SC and FS interneuron action potential times differed, with SC action potentials following a bimodal distribution with respect to the theta phase, whereas action potentials fired by interneurons followed a broad unimodal distribution ($p = 6 \times 10^{-4}$, NSOA) (Figures 1H and 1I). The frequency and relative timing of action potentials fired by SCs and interneurons, which we record here during optical theta stimulation, is similar to that recorded from neurons in layer II of the MEC during theta activity in behaving animals (Chrobak and Buzsáki, 1998; Hafting et al., 2008; Mizuseki et al., 2009).

Nested gamma oscillations may enable temporal codes that operate relative to the theta cycle to be superimposed upon firing rate codes (Buzsáki and Wang, 2012; Lisman, 2005). For temporal codes that require predictable reference signals (Fries, 2009; Lisman, 2005), multiplexing of rate and phase codes is likely to be particularly effective if gamma oscillations have clock-like consistency between consecutive theta epochs (Lisman, 2005), but it is not clear how this might be achieved. Surprisingly, we find that while the timing and number of spikes fired by stellate or inhibitory neurons differs between theta cycles, the timing of the gamma oscillations relative to the theta cycle is robust (cf. Figures 1G–1I, 2A, and 2B). To quantify the reliability of gamma oscillations, we compared the time of each gamma peak during a theta epoch with its average time across all epochs. In many cells, each gamma peak fell within a 5 ms window on the majority of theta cycles (Figure 2C). Similarly, even on the fifth gamma peak of each theta cycle, the difference between the time of each gamma peak and the time of the corresponding average peak could be <3 ms, compared with the gamma period of >10 ms (Figure 2D). For both measures, some, but not all, SCs demonstrate nested gamma activity

with timing that is consistent between theta cycles. While the reason for this variability is unclear, these observations nevertheless establish that in principle local theta drive to circuits in the MEC can generate gamma activity with clock-like properties in a substantial fraction of SCs.

To further compare the timing of optically induced nested gamma with activity in vivo, we averaged traces captured by triggering from the negative peak of each gamma oscillation. When nested gamma activity recorded from the MEC of behaving animals is analyzed in this way, average traces contain side peaks adjacent to the central peak, indicating periodicity of the gamma activity (Chrobak and Buzsáki, 1998). Applying this analysis to optically induced nested gamma also reveals side peaks adjacent to the central peak (Figure 2E). This comparison is consistent with the idea that theta-nested gamma oscillations in the entorhinal circuit provide a reference signal for hypothesized coding schemes that require precise temporal coordination of action potential firing (Buzsáki and Wang, 2012; Lisman, 2005).

To test whether the properties of nested gamma oscillations are unique to theta frequency stimulation, we compared responses to optical stimulation at 2, 8, and 16 Hz (Figure S2). With activation at 2, 8, and 16 Hz, we observed 23 ± 0.3, 6.6 ± 0.1, and 2.7 ± 0.2 oscillations per stimulus cycle ($p < 10^{-9}$, ANOVA). Although there is no difference in the frequency with maximum power for 2 Hz compared to 8 Hz stimulation ($p = 0.11$, ANOVA), gamma activity was not as consistently maintained through each 2 Hz cycle, with the result that the total number of gamma cycles available to contribute to information processing is reduced ($p = 0.0003$, t test). Thus, the phase of maximum gamma power occurred earlier in the stimulation cycle ($p = 0.0005$), the gamma frequency at the trough of the stimulation cycle was lower ($p = 0.005$, $n = 6$), and the gamma activity persevered through a narrower range of the stimulation cycle ($p = 1.1 \times 10^{-6}$). These properties did not differ between 8 Hz and 16 Hz stimulation ($p > 0.1$ for all comparisons). These data suggest that layer II of the MEC is optimized to generate gamma oscillations for approximately half the duration of each theta cycle but is less effective at sustaining gamma oscillations during stimulation at lower frequencies, while stimulation at higher frequencies generates fewer gamma oscillations per cycle.

Together, these data suggest that theta frequency activation of MEC layer II is sufficient to generate theta-nested gamma activity that resembles activity observed from the MEC of behaving animals (Chrobak and Buzsáki, 1998; Colgin et al., 2009; Lisman, 2005; Mizuseki et al., 2009). In both forms of nested activity, the frequency of gamma oscillations is similar, action potential firing by interneurons and excitatory neurons is on the same phase of the theta cycle, and on each theta cycle excitatory neurons fire relatively few spikes, whereas interneurons fire multiple spikes. Nested gamma activity has clock-like properties that may enable it to serve as a reference signal for temporal codes.

## Temporally Coordinated Feedback Inhibition Mediates Nested Gamma Oscillations

What circuit mechanisms mediate nested gamma oscillations? In principle, gamma frequency oscillatory activity can be generated exclusively by interneuron networks or by networks that involve coordination of action potential firing by interneurons and excitatory neurons (Buzsáki and Wang, 2012; Fries, 2009; Tiesinga and Sejnowski, 2009). The respective roles of these mechanisms in generating theta-nested gamma oscillations are not clear.

To establish whether synaptic input from excitatory or inhibitory cells is required for nested gamma oscillations, we blocked each component of synaptic transmission pharmacologically. Antagonists of ionotropic glutamate receptors (iGluRs) reduced total gamma power by a factor of 5.53 in SCs ($n = 23$, $p = 1.1 \times 10^{-8}$, paired t test) and a factor of 28.9 in FS interneurons ($n = 5$, $p = 4.4 \times 10^{-4}$, paired t test). As a result, spectral peaks at gamma frequencies were no longer observed (Figure 3). Antagonists of iGluRs had only very small effects on the mean firing rate (SCs: $p = 0.28$, $n = 24$, FS ints: $p = 0.04$, $n = 8$, paired t tests) and did not affect theta modulation of firing (Figure S3). The relatively small change in firing rate after block of iGluRs is because the majority of the current driving action potential firing is mediated directly by activation of ChR2 (Figure S3). Therefore, the absence of gamma frequency activity during block of iGluRs is not explained by failure of interneurons to generate action potentials during optical theta stimulation. Instead, these data indicate that excitatory synaptic transmission mediated by iGluRs is required to coordinate nested gamma frequency activity.

To determine whether theta-nested gamma is generated independently of synaptic connections from neurons in deeper layers of the MEC, and to further investigate differences between optical and pharmacologically induced gamma activity, we recorded from layer II neurons in slices in which the adjacent deeper layers of the MEC have been separated (Figures 3G and 3H). Blocking NMDA receptors abolishes pharmacologically induced gamma activity generated locally in layer II of the MEC and reveals lower-frequency activity that originates from layer III (Middleton et al., 2008). In contrast, we find that optical theta-nested gamma activity is generated in slices in which layers II and III are separated and is maintained after block of NMDA receptors with D-APV (Figures 3G and 3H). Therefore, optical theta-nested gamma is generated locally in layer II of the MEC and, unlike gamma induced pharmacologically in layer II, it does not require activation of NMDA receptors.

We next tested the role of fast inhibitory synaptic transmission. Antagonists of GABA receptors substantially reduced theta-nested gamma activity in SCs (by an average factor of 13.5, $p = 0.02$, $n = 8$, paired t test) (Figures 4A–4C). Block of synaptic inhibition had a small effect on the frequency ($p = 0.046$, $n = 8$, paired t test) but did not affect theta modulation of action potentials fired by SCs (Figure S4). Importantly, block of inhibitory synaptic transmission did not reveal excitatory inward currents in recordings from SCs during theta stimulation, even though SCs fired at 13.4 ± 2.7 Hz, suggesting that SCs do not form recurrent excitatory connections with one another. To further test this possibility, we drove SCs to fire action potentials using ramp stimuli (Figures 4D and 4E). Because the ramps switch SCs from silent to active states, we expect them to reveal synaptic responses that depress during prolonged stimulation or that summate from distal locations. Ramp stimuli also did not evoke detectable synaptic responses (Figures 4D and 4E

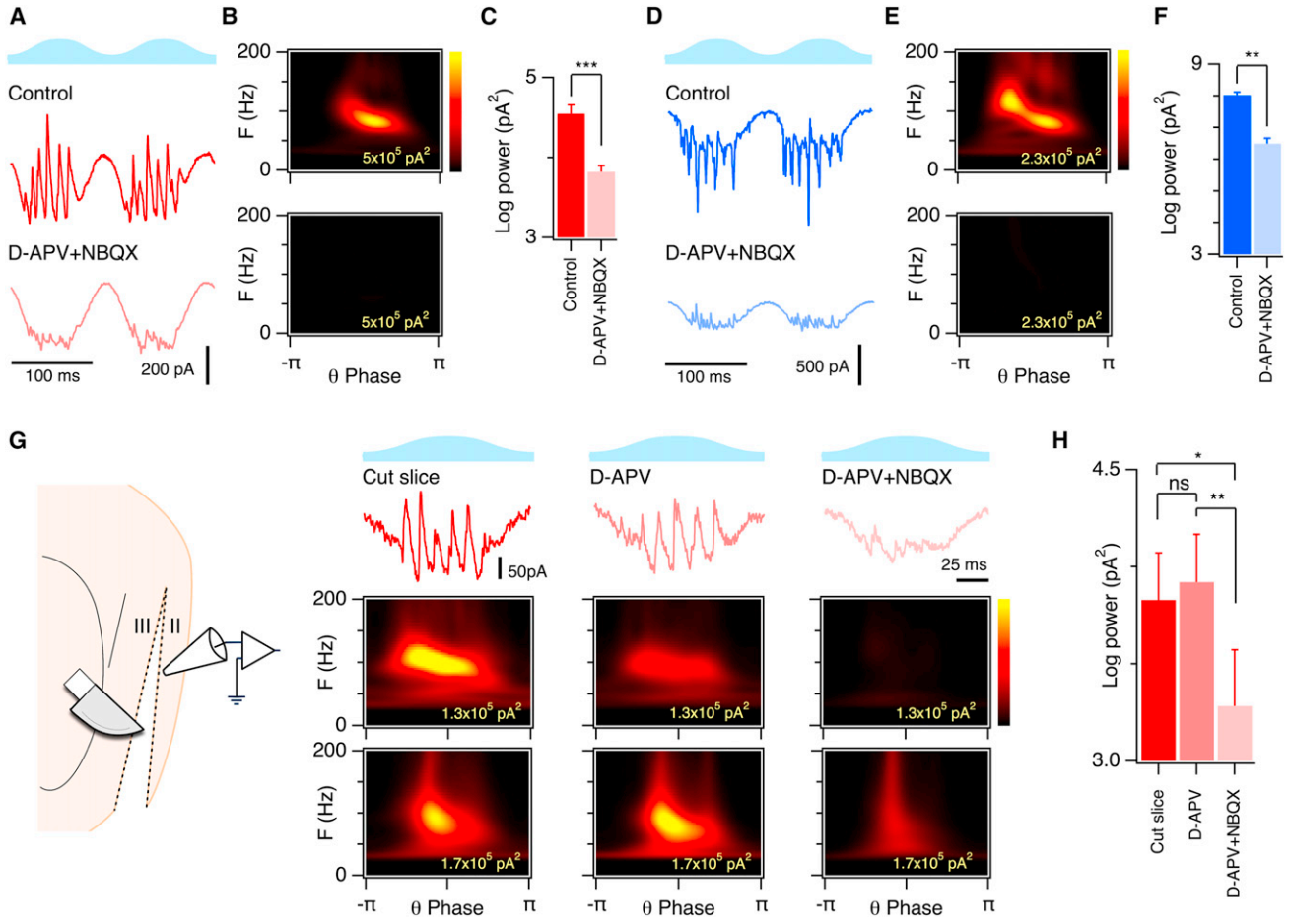


**Figure 3. Nested Gamma Oscillations Require Feedback Inhibition**

(A) Example of nested gamma frequency synaptic currents recorded from an SC before (control) and during block of iGluRs (NBQX + D-APV).

(B) Scalograms for all theta epochs from experiment in (A) in control (top) and after block of iGluRs with NBQX and D-APV (bottom), demonstrating that iGluRs are required for nested gamma activity.

(C) Mean data from all experiments indicating total power in control conditions and during block of iGluRs (n = 23, $p = 1.1 \times 10^{-8}$, paired t test). Data are log transformed to reduce the variance for statistical testing.

(D–F) Same as for (A–C) except that data are for FS interneurons. For (F), n = 5 and $p = 4.4 \times 10^{-4}$.

(G) Schematic indicates the slice cut to separate layers II and III (left). Examples of synaptic currents (row 2), corresponding scalograms (row 3), and the mean scalograms for all experiments (row 4), each plotted as a function of the phase of theta stimulation, demonstrate that nested gamma is maintained when connections between layers II and III are cut (control) and after subsequent block of NMDA receptors with 50 μM D-APV but is abolished by complete block of iGluRs.

(H) Mean power is not significantly different after block of NMDA receptors (p = 0.53, n = 6, paired t test) but is then reduced by complete block of iGluRs (p = 0.0015). Error bars in (C), (F), and (H) indicate SEM.

and Figure S4). Consideration of the numbers of SCs activated in these experiments indicates that the probability of connection between any two stellate cells is therefore likely to be considerably less than 1 in 500 (Figure S4 and Supplemental Experimental Procedures). These data indicate that nested gamma inputs to SCs originate from GABAergic interneurons and suggest that SCs do not form recurrent excitatory connections with one another.

To further understand the relationship between synaptic responses of SCs and FS interneurons, we examined their synaptic connections directly. Action potentials fired by SCs reliably triggered large excitatory synaptic responses in FS interneurons (Figures 4F, 4H, and 4I), while action potentials fired by FS interneurons triggered inhibitory synaptic responses in SCs (Figures 4G–4I). In contrast, action potentials in SCs did not generate synaptic currents in other simultaneously recorded SCs (Figures 4H and 4I), further supporting our conclusion that direct synaptic connections between SCs are rare or absent. The absence of excitatory synaptic connections between SCs is unlikely to result from our recording conditions, because in the slice preparation that we use axon collaterals from SCs are maintained (Garden et al., 2008), while excitatory synaptic transmission onto SCs and from SCs to other cells is clearly intact (see Figures 3 and 4 and Garden et al., 2008). Together with the

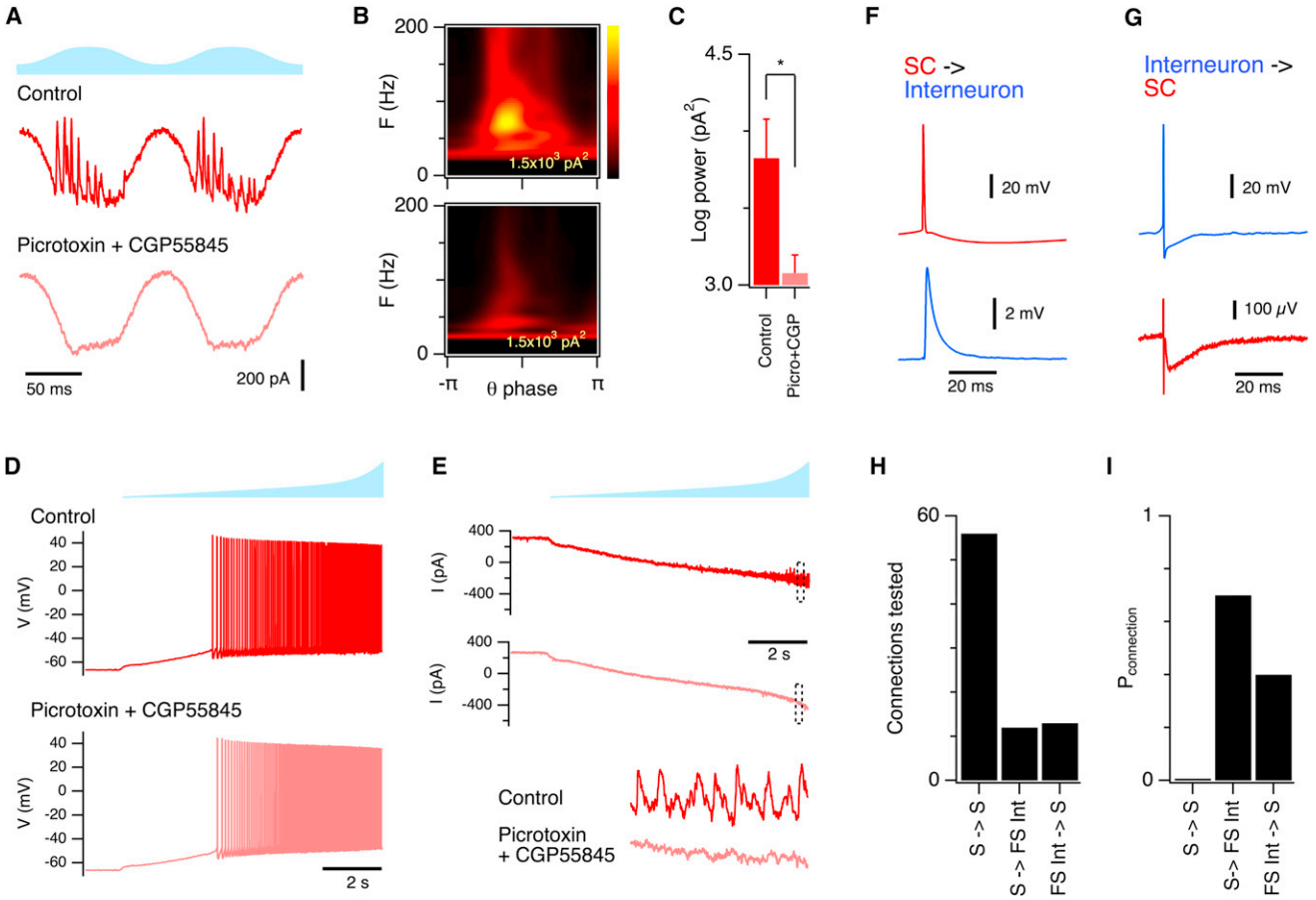


**Figure 4. Feedback Inhibition without Recurrent Excitation Mediates Interactions between Stellate Cells**

(A) Examples of membrane currents recorded from an SC during theta frequency network stimulation (top) in control conditions (middle) and during block of GABA receptors with picrotoxin (50 μM) and CGP55845 (1 μM) (bottom). Outward-going synaptic currents are abolished when GABA receptors are blocked. Even after block of inhibition, inward synaptic currents are not observed, indicating that SCs do not form excitatory connections to one another.

(B) Average scalogram of synaptic activity recorded from the SC in (A) before (top) and during (bottom) block of GABA receptors.

(C) Total power of the largest peak in the scalogram is reduced by block of GABA receptors (n = 8, p = 0.02). Error bars indicate SEM.

(D and E) Example of membrane potential (D) and current (E) of an SC during ramp-like optical activation of layer II in control conditions (top trace) and subsequently during block of GABA receptors (bottom trace). Although the optical stimulus drives action potential firing at high frequencies (D), excitatory synaptic currents are not observed (E), further indicating that SCs do not form direct synaptic connections with one another. Traces in the boxed regions in (E) are shown below on an expanded timescale.

(F) Example of synaptic response of an FS interneuron to an action potential in a simultaneously recorded presynaptic SC.

(G) Example of synaptic response of an SC to an action potential in a simultaneously recorded presynaptic FS interneuron.

(H and I) Number of pairs (H) and probability of functional connections for the pairs tested (I) for pairs of SCs (S -> S), presynaptic SC to postsynaptic FS interneuron (SC -> interneuron), and presynaptic FS interneuron to postsynaptic SCs (interneuron -> SC).

results of our optogenetic experiments, these data indicate a circuit architecture for nested gamma oscillations, and presumably layer II function in general, whereby SCs interact with one another indirectly via inhibitory interneurons and not through recurrent excitatory connections.

How is the precise timing of the nested gamma oscillations generated? The timing of gamma frequency synaptic currents was strongly correlated between SCs and FS interneurons, with excitatory input to interneurons preceding inhibitory input to SCs by 2.81 ± 0.59 ms (n = 8) (Figures 5A–5C). Synaptic currents were synchronized between pairs of nearby SCs with lag <1 ms, indicating that SCs receive common synchronizing drive from inhibitory neurons (n = 17) (Figure S5). Spikes fired by SCs and interneurons were more likely on the rising phase shortly after the trough of the gamma cycle but were not precisely locked to a particular gamma phase (Figures 5D–5F). The preferred firing phase of SCs was at +0.32 ± 0.02 radians relative to the trough of the synaptic gamma oscillation, whereas firing of FS interneurons was later at +0.85 ± 0.02 radians (p = 0.002, n = 48 SCs, n = 11 interneurons, NSOA). Therefore, excitatory SCs fire near the trough of each gamma cycle just as during exploratory behavior (Chrobak and Buzsáki, 1998). This rapidly triggers spiking by FS interneurons, which then reduces the probability of SC firing until the trough of the next gamma cycle.

Together, these data suggest that coordinated timing of action potentials fired by SCs and FS interneurons mediates

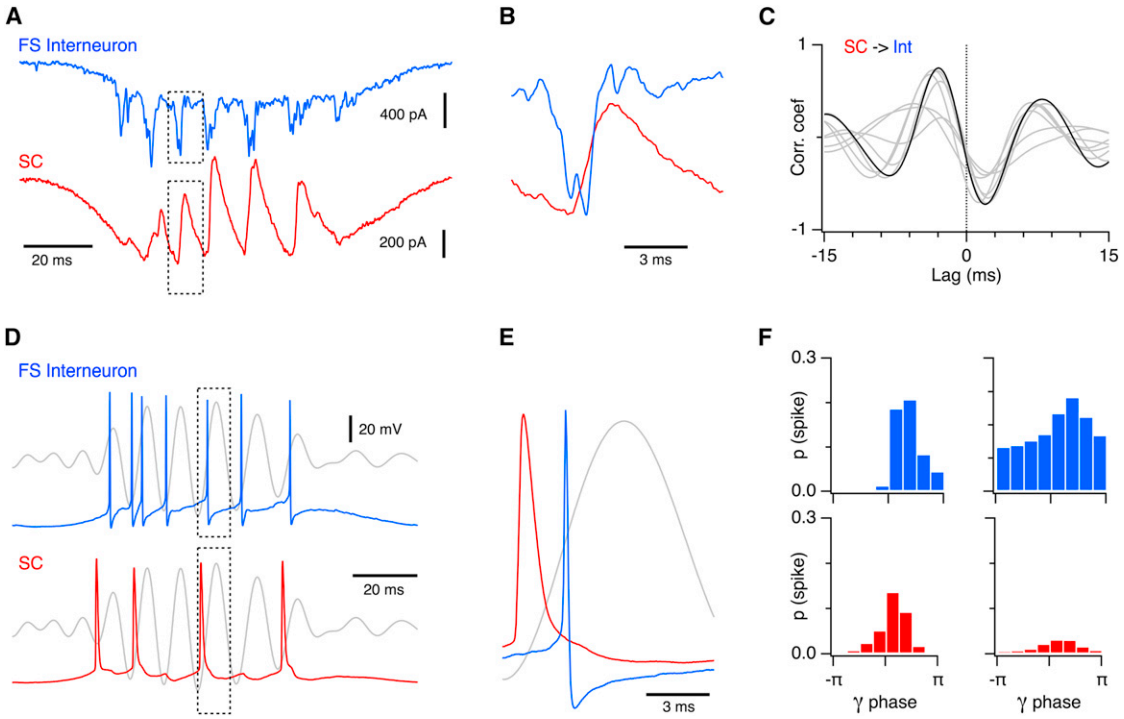


**Figure 5. Temporal Organization of Synaptic Events and Action Potential Activity during Nested Gamma Oscillations**

(A) Example of synaptic currents recorded simultaneously from an FS interneuron and an SC during a single cycle of theta frequency stimulation.

(B) Detail of regions in (A), indicated by the box, demonstrates that excitatory input to interneurons arrives before inhibitory input to SCs.

(C) Cross-correlation between SC and FS interneuron membrane currents during theta stimulation for the example in (A and B) and for seven other experiments indicates that excitation to interneurons consistently leads inhibition to SCs (maximum correlation = 0.56 ± 0.07, lag = 2.81 ± 0.59 ms, n = 8).

(D) Example of a simultaneously recorded FS interneuron, SC, and extracellular field potential during a single epoch of theta stimulation.

(E) Detail from (D) illustrating action potential initiation in the stellate cell earlier in the gamma cycle and preceding action potential initiation in the FS interneuron.

(F) The probability of action potential initiation as a function of phase of the local field potential gamma signal for interneurons (top) and SCs (bottom) for the example recordings in (D and E) (left) and on average for all recordings (right).

theta-nested gamma oscillations. This is distinct from pharmacological models of gamma activity in the MEC in which the frequency of excitatory drive to interneurons is less than the network gamma frequency (Cunningham et al., 2003) and in which NMDA receptor activation is required for oscillations generated within layer II (Middleton et al., 2008). Instead, subsets of SCs firing before the trough of each gamma cycle generate excitatory postsynaptic currents in FS interneurons. Action potential firing by FS interneurons then generates feedback inhibition onto SCs. While previous in vivo recordings are consistent with this mechanism (Buzsáki and Wang, 2012), because these experiments were correlative they do not enable synaptic mechanisms to be tested directly. The strength of our approach combining optogenetic and pharmacological manipulation is highlighted by our evidence that, in contrast to previous suggestions based on less direct methods (Beed et al., 2010; Kumar et al., 2007; Quilichini et al., 2010), the primary mechanism for communication between SCs is via inhibitory interneurons.

## Feedback Inhibition Enables Generation of Grid Fields and Nested Gamma Oscillations

To establish whether the synaptic connectivity deduced from our experiments can account for nested gamma activity and for generation of grid firing fields, we developed a network model based on our data (Experimental Procedures and Figure S6). Grid firing fields can be generated by networks that produce attractor states (Burak and Fiete, 2009; Fuhs and Touretzky, 2006; Guanella et al., 2007; McNaughton et al., 2006) but, except for a model containing exclusively inhibitory interneurons (Burak and Fiete, 2009), previous models rely on direct connections between excitatory cells. This is inconsistent with our finding that SCs communicate primarily via inhibitory interneurons. Previous models also do not generate nested gamma activity. We therefore simulated networks in which excitatory SCs only communicate with one another indirectly via inhibitory neurons, while theta-modulated excitatory afferents target both neuron types.

We initially considered a network configuration in which the strongest synapses from inhibitory neurons are onto adjacent excitatory cells, while the strongest connections from excitatory cells are onto a surrounding ring of inhibitory neurons (E-surround configuration) (see Experimental Procedures and Figure S6). This network, which has connectivity consistent with our experimental data, generates persistent attractor states (Figure 6A). Attractor states in the network are stable during theta stimulation (Figure 6B) and coexist with theta-nested gamma

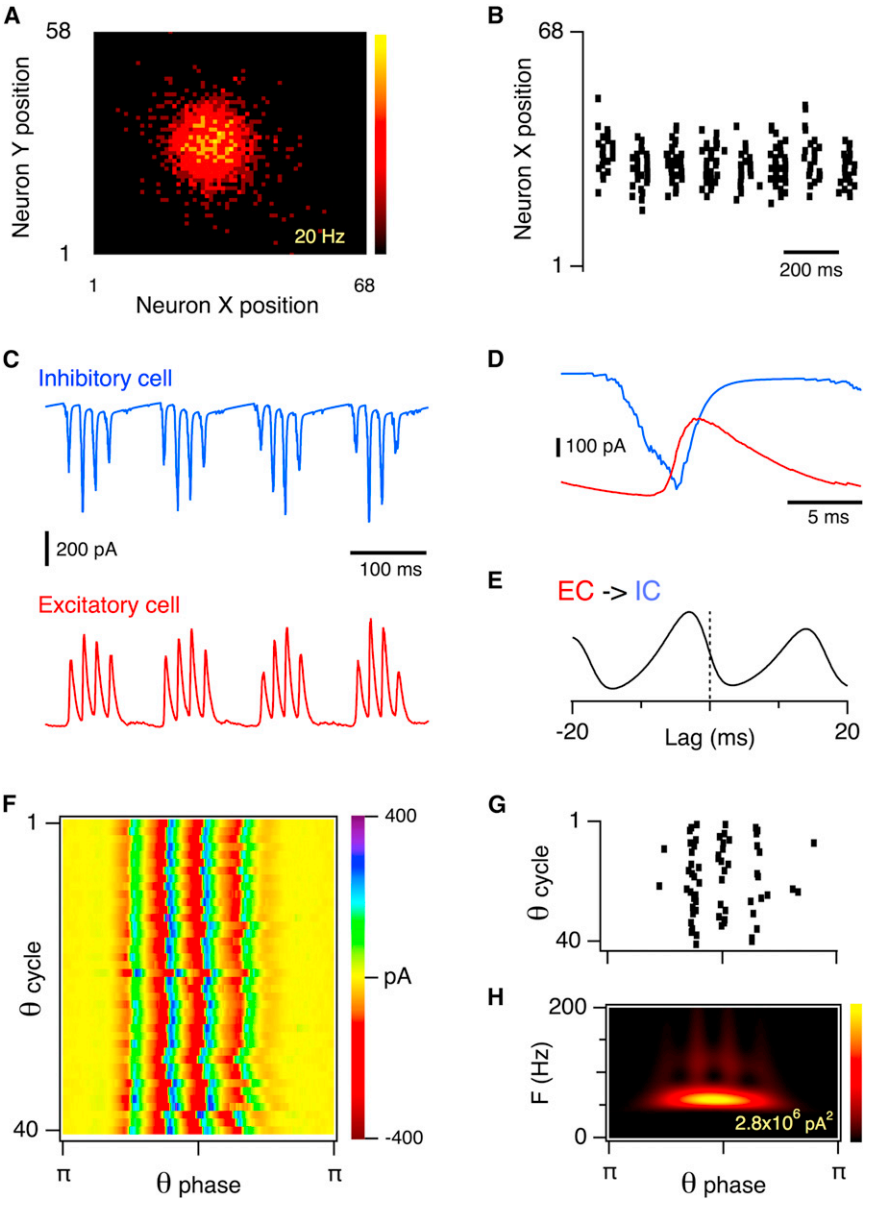


**Figure 6. Clock-like Nested Gamma Oscillations Are Generated by Attractor Networks of Neurons Connected Only through Recurrent Inhibition**

(A) A snapshot of neuronal activity as a function of position in the 68 × 58 layer of excitatory neurons. Data in this figure are from the network in the E-surround configuration, but similar results are obtained using the I-surround configuration.

(B) Spike rasters from 68 neurons corresponding to row 29 in (A), indicating stability of the bump during successive theta cycles.

(C) Examples of synaptic currents recorded from inhibitory and excitatory neurons at the center of the activity bump in (A).

(D and E) Synaptic currents during a single gamma cycle (D), and the cross-correlation between synaptic currents recorded from excitatory and inhibitory neurons (E), illustrate how excitatory input to interneurons precedes inhibitory input to excitatory neurons. Both examples are from the neuron pair in (C).

(F) Synaptic currents from 40 consecutive theta cycles plotted on a color scale indicate the consistent timing of nested gamma oscillations across theta cycles. Data are from an excitatory neuron at the center of the activity bump in the model network described in (A–E). Similar clock-like nested gamma responses are observed from neurons at all locations.

(G) Action potential rasters for a cell at the center of the bump as in (F) for 40 consecutive theta epochs. The timing, but not the number of action potentials, is similar on each theta cycle.

(H) Example scalogram of membrane current power during 40 consecutive theta cycles for the neuron in (F and G).

frequency synaptic oscillations strikingly similar to our experimental data (Figures 6C–6H). Comparing gamma activity in consecutive theta epochs, we find that, as in the experimental data, the gamma signal is clock-like (Figure 6F). The timing of synaptic excitation and inhibition (Figures 6C–6E, 6G, and 6H) is also similar to experimentally induced theta-nested gamma oscillations (cf. Figures 2, 3, 4, and 5). These simulations demonstrate that feedback inhibition is sufficient to generate network attractor states while also accounting for theta-nested gamma oscillations of activity in the MEC.

We next asked whether networks in which excitatory cells communicate only via inhibitory interneurons generate grid firing fields when movement is simulated. Because grid-like firing fields are generated by integration of self-motion signals (Fuhs and Touretzky, 2006; Guanella et al., 2007; McNaughton et al., 2006), we connected synaptic inputs encoding speed of movement in particular directions to subsets of either excitatory or inhibitory neurons (see Experimental Procedures). These inputs move the bump of active neurons according to movement of the animal. Because input from the hippocampus to the MEC is necessary for generation of grid firing fields (Fyhn et al., 2004), a place cell input was also connected to the excitatory cells in the network (Guanella et al., 2007). This input was organized so that place cells project to grid cells that are active at the same location. In the simulations we describe here, this input is active only for 100 ms every 10 s so that spatial firing is determined primarily by integration of the velocity inputs and the place cell input functions to oppose drift in the attractor state.

When velocity inputs are targeted to excitatory neurons, the network tracks a wide range of movement velocities and generates grid fields when provided with realistic movement trajectories (Figures 7A and 7B). When velocity inputs target interneurons, the range of movement velocities that can be tracked is more restricted (Figure 7A), but grid fields are nevertheless indistinguishable from the control network ($p = 0.25$, t test comparing

gridness scores) (Figure 7B). Consistent with experiments in which the hippocampus is lesioned (Fyhn et al., 2004), after removal of the place cell input to the model, grid fields are no longer apparent because of drift in the attractor state ($p = 2.0 \times 10^{-9}$, t test) (Figures 7C and S7). This drift may result from noise in the network or from the network architecture (Welinder et al., 2008). When the place cell input is activated more frequently, as is likely to be the case in vivo, the network continues to generate grid fields (data not shown). Together, these data establish that theta-modulated attractor networks connected by feedback inhibition are sufficient to generate grid fields. They predict that velocity inputs can effectively target excitatory SCs or inhibitory interneurons and that hippocampal input is required to prevent spontaneous drift in the attractor state.

We next used the model to investigate the relationship between theta activity and grid cell firing. When theta-modulated input to the model is replaced by a constant drive of similar mean amplitude, grid fields are maintained ($p = 0.43$ versus control gridness score) (Figures 7D and S7). Models containing exclusively inhibitory interneurons also rely on a constant tonic excitatory drive to generate grid fields and therefore lead to a similar prediction (Burak and Fiete, 2009). This is consistent with the observations that grid fields are present in the absence of theta activity (Yartsev et al., 2011) and that only a subset of grid cells have firing that is modulated at theta frequency (Krupic et al., 2012). It also suggests that abolition of grid fields after septal lesions (Brandon et al., 2011; Koenig et al., 2011) may be due to loss of both an external drive to the network and its theta modulation, in which case the network model also fails to generate grid fields (data not shown).

While inhibitory neurons alone are sufficient to represent location (Burak and Fiete, 2009), our experimental data indicate that inhibitory and excitatory neurons must integrate signals they receive from one another. Models that incorporate only one neuron type do not specify how this is done, whether firing fields of interneurons and excitatory neurons differ or if variations in connectivity lead to different predictions for spatial firing or nested gamma activity. We therefore investigated the firing properties of inhibitory neurons and the consequences of different organizations of connections between excitatory and inhibitory neurons. We find that inhibitory neurons in the E-surround network configuration encode location (Figure 7F). However, unlike in models containing only inhibitory neurons (Burak and Fiete, 2009), interneurons in the E-surround network have inverted grid fields (Figure 7F). We next investigated networks in which the strongest inhibition is onto a ring of excitatory SCs, but the strongest excitation is local (I-surround configuration) (Figure 7E). Excitatory neurons in this configuration also have grid fields and theta-nested gamma oscillations in their synaptic input (Figures 7G and S7). In this configuration, interneurons have grid fields that are similar to those of excitatory cells (grid score $1.07 \pm 0.01$ and $1.08 \pm 0.01$ for excitatory and inhibitory cells respectively, $p = 0.78$, t test). Multiple peaks in the two-dimensional (2D) Fourier transform of grid fields recorded in behaving animals could indicate that spatial firing originates from upstream band cells rather than from an attractor network of the kind we characterize here (Krupic et al., 2012). However, in both model configurations, 2D Fourier spectrograms of the firing field have multiple peaks even though band cells are not found in either configuration, indicating that these peaks do not necessarily imply the existence of upstream band cells (Figures 7B, 7D, 7F, and 7G). We nevertheless found that leaving intact only one direction of velocity input to either network leads to emergence of band cells (Figure S7). In this case, both networks continue to generate theta-nested gamma oscillations. Together, these data indicate that theta-nested gamma oscillatory activity is a general feature of attractor networks that generate representations of space using indirect inhibitory interactions between excitatory cells. They also demonstrate that the nature of spatial representation by interneurons depends on the organization of connections within the network.

Our simulations lead to a number of predictions about the membrane potential dynamics of SCs during behavior (Figure 8). Theta-nested gamma frequency synaptic activity is found in both neuron types in E- and I-surround configurations of the model (Figures 8B, 8C, 8G, 8H, 8L, and 8M). In both model configurations, excitatory neurons fire action potentials soon after the trough of gamma (Figure 8D), while firing by interneurons is typically later in the gamma cycle (Figures 8I and 8N). Inhibition to SCs and excitation to interneurons varies as a function of distance from the center of the firing field ($R^2 = 0.61$, $p < 10^{-9}$ and $R^2 = 0.63$, $p < 10^{-9}$, respectively, for the E-surround model and $R^2 = 0.66$, $p < 10^{-9}$ and $R^2 = 0.63$, $p < 10^{-9}$ for the I-surround model) (Figures 8E, 8J, and 8O). In all configurations, the synaptic drive to excitatory and inhibitory neurons coincides with the depolarizing component of the theta input and the amplitude of the gamma frequency inhibitory input to SCs is greatest outside the firing field and weakest at the center of the firing field. However, in the E-surround configuration, gamma frequency excitation of interneurons is strongest on the edges of the inverted firing field and weakest at the center (Figures 8G, 8H, and 8J). In contrast, in the I-surround configuration, this relationship is reversed (Figures 8L, 8M, and 8O). Together, these data predict that in individual grid cells the amplitude of theta-nested gamma depends on an animal's location.

## DISCUSSION

We demonstrate that theta frequency activation of layer II of the MEC generates nested gamma frequency oscillations that resemble activity observed during spatial behaviors. We find that feedback inhibition is the primary mode of communication between SCs and is sufficient to account for nested gamma oscillations. While the activity of individual neurons varies between gamma cycles, coordination of synaptic inhibition and excitation nevertheless results in gamma oscillations with clock-like timing suitable for use as a reference signal in temporal codes. We show that feedback inhibition is also sufficient for emergence of attractor states that coexist with nested gamma oscillations and that generate rate-coded grid firing fields. Therefore, grid firing fields and theta-nested gamma oscillations may result from a common local circuit architecture, which is defined by communication between SCs mediated primarily via inhibitory interneurons.

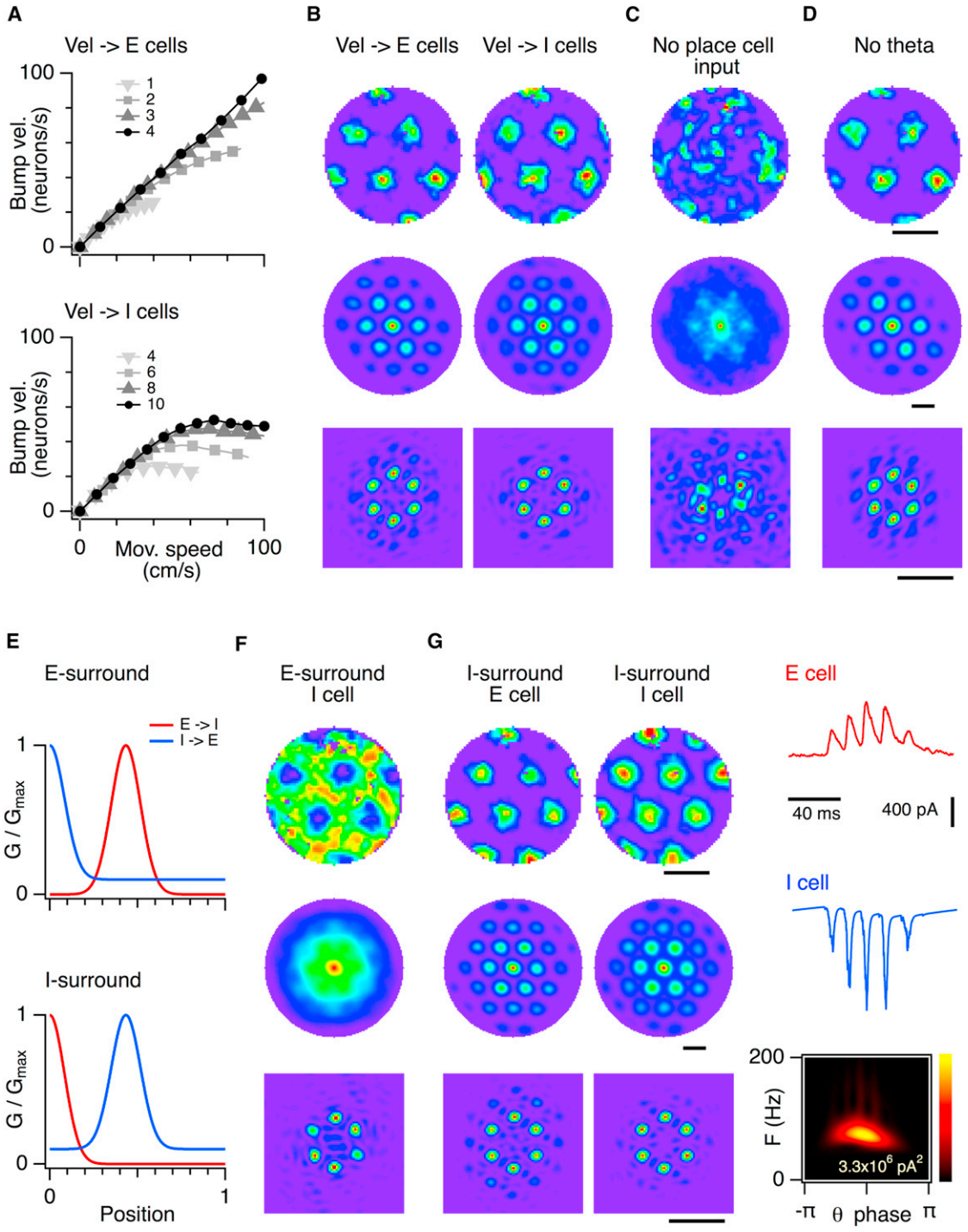


**Figure 7. Theta-Nested Gamma Oscillations Coexist with, but Are Not Necessary for, Grid Firing Fields**

(A) Speed of movement of the attractor bump is plotted as a function of the amplitude of the input encoding movement velocity for networks with differing offset in the outgoing connection profile from excitatory to inhibitory cells. Networks in which movement velocity drives excitatory neuron firing (top) maintain a wider linear response range than networks in which movement inputs are targeted to interneurons.

(B) Example heat maps for firing (top), corresponding autocorrelation plots (middle), and 2D Fourier spectrograms (bottom) generated by simulated exploration of the arena using attractor models with velocity input to excitatory cells (left) or inhibitory cells (right). Gridness scores do not differ between networks with velocity input to excitatory neurons (E cells) (1.1 ± 0.01, n = 10) and inhibitory neurons (I cells) (1.12 ± 0.01, n = 10, p = 0.25).

(C) Simulation in the absence of place input. The firing fields have a gridness score of 0.22 ± 0.07, which is substantially less than that of control neurons ($p = 1.16 \times 10^{-9}$, n = 15), indicating that grid firing is absent.

*(legend continued on next page)*

The optically induced nested gamma activity that we describe here has key features in common with theta-nested gamma oscillations observed during spatial exploration. These include a similar frequency (60–100 Hz) (Chrobak and Buzsáki, 1998; Colgin et al., 2009), activation of FS interneurons and excitatory cells at similar phases of the theta oscillation (Chrobak and Buzsáki, 1998; Mizuseki et al., 2009), and similar timing of action potentials relative to the nested gamma oscillation (Chrobak and Buzsáki, 1998). Both forms of theta-nested gamma activity appear to be mechanistically distinct from pharmacologically induced gamma oscillations, which have much lower frequency (30–45 Hz), no clear relationship to theta activity, and different involvement of NMDA receptors (Cunningham et al., 2003; Dickson et al., 2000; Middleton et al., 2008; van Der Linden et al., 1999). Signatures of clock-like activity found during optical theta-nested gamma (Figure 2) are also apparent during in vivo theta-nested gamma activity (Chrobak and Buzsáki, 1998), indicating that circuits in layer II of the MEC contain cellular machinery to generate reference signals for temporal coding (Buzsáki and Draguhn, 2004; Lisman, 2005).

Understanding brain computations requires knowledge of the wiring of neuronal circuits. In many cortical areas, including deeper layers of the MEC (Dhillon and Jones, 2000), information is transmitted directly between nearby excitatory neurons (Deuchars et al., 1994; Mason et al., 1991; Song et al., 2005). Axons of SCs have collaterals in layer II of the MEC (Burgalossi et al., 2011; Garden et al., 2008; Quilichini et al., 2010), which have been suggested to form recurrent excitatory connections (Beed et al., 2010; Kumar et al., 2007). However, we did not observe excitatory synaptic responses when large populations of SCs fire action potentials (Figures 4A and S4), indicating that SCs in layer II of the MEC do not communicate directly with one another. This is consistent with recordings from pairs of SCs (Figures 4F–4I and Dhillon and Jones, 2000). By demonstrating connections in both directions between SCs and interneurons, our data instead indicate that communication between SCs in layer II of the MEC is primarily through feedback inhibition.

Because SCs in layer II of the MEC are likely to be grid cells (Burgalossi et al., 2011; Canto et al., 2008; Pastoll et al., 2012a), elucidation of their local connectivity and their role in oscillatory network activity is critical to understanding grid firing fields. Our finding that SCs communicate primarily by feedback inhibition argues against models that rely on direct excitation between grid cells (Fuhs and Touretzky, 2006; Guanella et al., 2007; Navratilova et al., 2012). Instead, it supports the theoretical prediction that inhibition can mediate grid firing fields (Burak and Fiete, 2009) but suggests that this is implemented using interactions between inhibitory interneurons and SCs rather than through direct inhibitory connections between grid cells. Nevertheless, while our model establishes the sufficiency of inhibitory feedback for generation of attractor states by SCs, the actual network may depend on interactions between layers for its functionality, while other details of the model that enable it to generate spatial representations are not yet well constrained. For example, in our model, velocity and theta inputs target grid cells directly, but they could also arrive indirectly via neurons in deeper layers of the MEC (Navratilova et al., 2012).

By exploring models in which SCs communicate solely by feedback inhibition, we make several predictions. First, interneurons may have spatial firing fields. An E-surround network configuration causes interneurons to have inverted grid firing fields, whereas an I-surround configuration causes interneurons to have fields with grid scores similar to excitatory neurons (Figure 7). Consistent with these predictions, interneurons with spatial firing fields defined by a decrease in firing frequency have been identified in the hippocampus (McNaughton et al., 1983; Wilent and Nitz, 2007), although to our knowledge spatial firing has not been investigated for entorhinal interneurons. Second, the role of theta frequency input can be dissociated into a tonic drive, which is required for grid cell firing, and phasic theta modulation of that drive, which is required for generation of clock-like nested gamma oscillations (Figure 7E). This is consistent with previous data (Brandon et al., 2011; Koenig et al., 2011; Yartsev et al., 2011), but it remains to be tested directly. Third, recording of the membrane potential of SCs in behaving animals should reveal gamma frequency inhibitory postsynaptic potentials on the depolarizing phase of theta with amplitude that decreases with distance from the center of the firing field (Figure 8). In contrast, recording from FS interneurons should reveal gamma frequency excitatory postsynaptic potentials on the depolarizing phase of theta with amplitude relative to the firing field that depends on whether the network has an E-surround or an I-surround configuration (Figure 8). While our model is no doubt considerably simplified compared to the layer II network in behaving animals, experimental corroboration of these predictions would lend strong support to the architecture that we outline here as a basis for generation of grid firing fields.

What is the function of theta-nested gamma oscillations? Our results suggest a cellular substrate for several theories of temporal coding. First, nested gamma oscillations may enable coincident firing of ensembles of SCs within time windows required for coincidence detection by downstream neurons in the dentate gyrus (Buzsáki and Wang, 2012; Chrobak and Buzsáki, 1998). Second, phase locking of nested gamma oscillations between different regions may control the efficacy of their interactions with up- or downstream networks (Buzsáki and Wang,

(D) Simulations in which theta frequency modulation of network drive is removed. Grid fields have a gridness score of 1.11 ± 0.01 and are similar to control grid fields (n = 10, p = 0.43).
(E) Synaptic conductance is plotted as a function of distance between neurons normalized to the size of the neurons' sheet for connections from E cells to I cells (excitation) and from I cells to E cells (inhibition) for E-surround (top) and I-surround (bottom) versions of the model.
(F) Predicted interneuron firing fields for the E-surround model configuration. The field appears as an inverted grid field such that the grid apex has a low firing rate and the region between the apices is coded by a high firing rate.
(G) Firing rate maps (top), spatial autocorrelations (middle), and 2D Fourier spectrograms (bottom) for example excitatory (left) and inhibitory (middle) neurons in the I-surround configuration. This network configuration also generates theta-nested gamma activity illustrated by synaptic currents during a single theta cycle and the scalogram of the inhibitory currents as a function of theta cycle phase (right).
Scale bars represent 60 cm for the rate and autocorrelation plots and 4 $m^{-1}$ for the Fourier spectrograms.

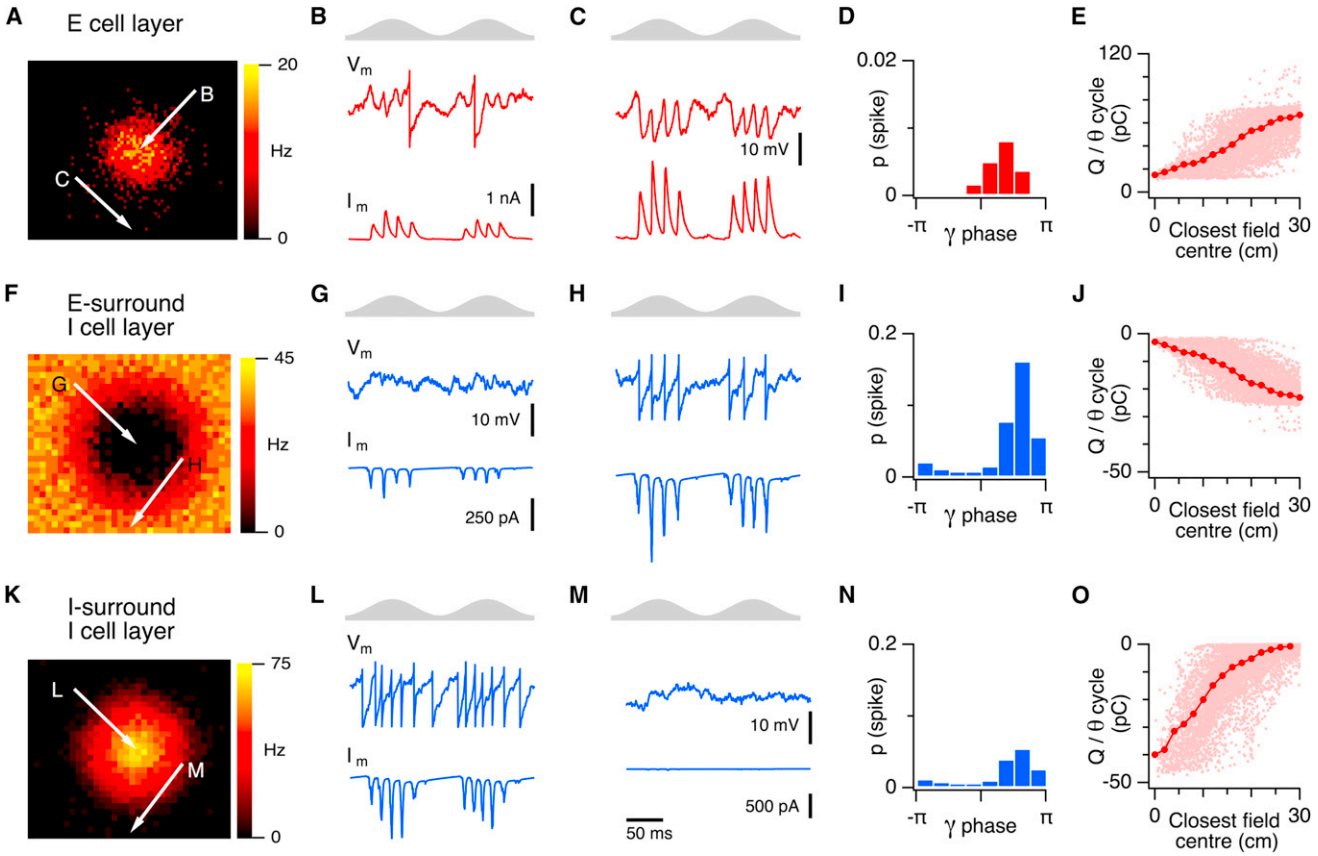


**Figure 8. Predicted Membrane Potential and Current Dynamics Associated with Grid Firing Fields**

(A) Location of the exemplar neurons in the excitatory cell layer with respect to the activity bump. Each color-coded point represents the firing frequency of a single neuron. Network is in the E-surround configuration, but results for excitatory cells are similar in the I-surround configuration.

(B and C) Membrane potential and current during two theta cycles for neurons at the locations indicated in (A). Both neurons received nested gamma frequency inhibitory input, but this is lower at the center of the bump, enabling the external theta drive to trigger action potential firing.

(D) Spike probability as a function of gamma phase for the excitatory neurons.

(E) Total charge during each theta cycle of the inhibitory synaptic input to an excitatory cell plotted as a function of distance from the center of the excitatory cell's nearest grid firing field during that cycle.

(F) Location of the exemplar neurons in the inhibitory cell layer in the E-surround network configuration. The activity bump is inverted with respect to the excitatory cell layer.

(G and H) Membrane potential and current during two theta cycles for neurons at the locations indicated in (F). Both neurons received nested gamma frequency excitatory input, but this is lower for interneurons that project onto excitatory cells at the center of the bump.

(I) Spike probability as a function of gamma phase for the inhibitory neurons.

(J) Total charge during each theta cycle of the excitatory synaptic input to an inhibitory cell plotted as a function of distance during that cycle from the center of the nearest grid firing field of the excitatory cell to which the inhibitory neuron makes strongest connections.

(K–O) Same as for (F–J) except for a network in the I-surround configuration. Bold points in (E), (J), and (O) indicate mean; SEM is smaller than the point size.

2012; Fries, 2009). In this scenario, temporal codes require that interacting brain areas generate theta-nested gamma activity of a similar frequency, with the gain of the interaction depending on the relative phases of the gamma activity. Third, nested gamma oscillations may be used in more complex schemes for temporal encoding of sequences in which distinct information is encoded within each gamma cycle (Lisman, 2005). This may include theta phase precession of action potentials for which the role of gamma activity is not yet clear (Lisman, 2005). While generation of gamma oscillations alone is sufficient for the first coding scheme, the other schemes rely on precise temporal relationships between theta and gamma (Buzsáki and Wang, 2012). Different properties of gamma activated by different frequencies of optical stimulation may reflect optimization of the circuit for these coding schemes (Figure S2).

In conclusion, our data provide evidence that feedback inhibition accounts for two well-established features of network activity in behaving animals. Our experiments and model recapitulate defining features of theta-nested gamma activity that is observed from neurons in the MEC and other brain areas (Chrobak and Buzsáki, 1998; Colgin et al., 2009; Lisman, 2005; Mizuseki et al., 2009). We establish that the circuit elements that produce gamma oscillations phase locked to theta can do so with remarkable trial-to-trial consistency, suggesting that the

local MEC circuit has clock-like properties required for reference signals for neuronal computations that rely on the timing of gamma oscillations (Buzsáki and Wang, 2012; Fries, 2009; Lisman, 2005). The simple principles for organization of the MEC circuit derived from these experiments also account for generation of grid-like firing fields. These results suggest that common circuit mechanisms evolved to support simultaneous rate and temporal coding in the CNS.

## EXPERIMENTAL PROCEDURES

### Electrophysiological Recordings

All experiments used adult (7- to 9-week-old) mice from Thy1-ChR2-YFP line 18 (Arenkiel et al., 2007). Sagittal brain slices were prepared and whole-cell patch-clamp recordings made as described previously (Garden et al., 2008; Pastoll et al., 2012b). The slices include all layers and the full dorsal-ventral extent of the MEC. Illumination for activation of ChR2 was from a 470 nM collimated LED (Thorlabs) introduced through the epifluorescence port of the microscope (Olympus BX-51) and focused onto the slice from above (Figure S1). The region of neurons activated by light had a radius of approximately 100 μm. Pharmacological agents were bath applied to the whole slice.

### Attractor Network Model

A network of exponential integrate and fire neurons (Fourcaud-Trocmé et al., 2003) was implemented using the Brian simulator (Goodman and Brette, 2008). Full details of parameter values and explanation of the model are in the Supplemental Experimental Procedures.

In the model, each neuron received an external current source composed of the sum of constant background activation, theta-modulated current simulated as cosine function, velocity modulation current, and hippocampal place field input. To simulate noise, we injected independent Gaussian-distributed current to give a 2 mV SD in the resting membrane potential of each neuron.

#### *Network Topology and Connectivity*

The network consisted of 68 × 58 excitatory cells and 34 × 30 interneurons uniformly distributed on a twisted torus (Guanella et al., 2007). In the E-surround configuration, connections from excitatory to inhibitory cells used AMPA- and NMDA-type conductances and their topography followed a ring-like organization with an appropriate offset for implementation of velocity modulation, while the topography of inhibitory to excitatory connections had a Gaussian profile (Figures S6A and S6B, Figure 7E). In the I-surround configuration, the topography of the excitatory to inhibitory connections followed the Gaussian profile, while the connections from inhibitory to excitatory neurons followed the ring-like organization.

#### *Velocity Modulation*

To perform path integration, the activity in the network must propagate along the direction of the simulated movement of the animal (Fuhs and Touretzky, 2006; Guanella et al., 2007; McNaughton et al., 2006). This is achieved by shifting the center of the synaptic profile of neurons in one of the populations (excitatory or inhibitory) in the direction of preferred movement. Each neuron was assigned a directional vector from a group of four directions (up, down, left, and right) and its outgoing synaptic weight profile was shifted by a predefined constant. During simulated movement, a velocity-modulated current was then injected into the neuron (Figure S6C). To evaluate spatial representation by the network during exploration, we simulated 15–20 min of movement. At each time point, the velocity vector was estimated as a forward difference of published positional data (Hafting et al., 2005).

#### *Place Cell Input*

Because action potential firing and noise lead to slow drift in the state of the network, unless otherwise stated, simulations contain an allothetic input from place cells that is active for 100 ms every 10 s and opposes the drift.

### Data Analysis and Statistics

Electrophysiology and simulation data were analyzed using built-in and custom routines in IGORpro, MATLAB, or Python. Comparisons between groups used ANOVA and Student's t test as indicated. For simulations, networks receiving a theta input and velocity modulation of the excitatory cells are considered as the control group. Gridness scores are calculated following previous studies (Sargolini et al., 2006). Full details for analysis of oscillatory and grid activity are given in the Supplemental Experimental Procedures.

## SUPPLEMENTAL INFORMATION

Supplemental Information includes seven figures and Supplemental Experimental Procedures and can be found with this article online at http://dx.doi.org/10.1016/j.neuron.2012.11.032.

## ACKNOWLEDGMENTS

This work was supported by the Biotechnology and Biological Sciences Research Council (M.F.N.), the Engineering and Physical Sciences Research Council (H.P. and L.S.), and the Commonwealth Scholarships Commission (H.P.). We thank Ian Duguid for comments on the manuscript and Patrick Kaifosh for suggestions about network configurations. This work made use of resources provided by the Edinburgh Compute and Data Facility. H.P. contributed to design of the study and performed and analyzed experiments. L.S. contributed to design of the study and performed and analyzed simulations. M.C.W.v.R. contributed to design of the study and analysis of simulations. M.F.N. designed and supervised the study, contributed to data analysis, and wrote the manuscript.

Accepted: November 30, 2012
Published: January 9, 2013

## REFERENCES

Arenkiel, B.R., Peca, J., Davison, I.G., Feliciano, C., Deisseroth, K., Augustine, G.J., Ehlers, M.D., and Feng, G. (2007). In vivo light-induced activation of neural circuitry in transgenic mice expressing channelrhodopsin-2. Neuron *54*, 205–218.

Beed, P., Bendels, M.H., Wiegand, H.F., Leibold, C., Johenning, F.W., and Schmitz, D. (2010). Analysis of excitatory microcircuitry in the medial entorhinal cortex reveals cell-type-specific differences. Neuron *68*, 1059–1066.

Brandon, M.P., Bogaard, A.R., Libby, C.P., Connerney, M.A., Gupta, K., and Hasselmo, M.E. (2011). Reduction of theta rhythm dissociates grid cell spatial periodicity from directional tuning. Science *332*, 595–599.

Burak, Y., and Fiete, I.R. (2009). Accurate path integration in continuous attractor network models of grid cells. PLoS Comput. Biol. *5*, e1000291.

Burgalossi, A., Herfst, L., von Heimendahl, M., Förste, H., Haskic, K., Schmidt, M., and Brecht, M. (2011). Microcircuits of functionally identified neurons in the rat medial entorhinal cortex. Neuron *70*, 773–786.

Buzsáki, G. (2002). Theta oscillations in the hippocampus. Neuron *33*, 325–340.

Buzsáki, G., and Draguhn, A. (2004). Neuronal oscillations in cortical networks. Science *304*, 1926–1929.

Buzsáki, G., and Wang, X.J. (2012). Mechanisms of gamma oscillations. Annu. Rev. Neurosci. *35*, 203–225.

Canolty, R.T., and Knight, R.T. (2010). The functional role of cross-frequency coupling. Trends Cogn. Sci. *14*, 506–515.

Canto, C.B., Wouterlood, F.G., and Witter, M.P. (2008). What does the anatomical organization of the entorhinal cortex tell us? Neural Plast. *2008*, 381243.

Chrobak, J.J., and Buzsáki, G. (1998). Gamma oscillations in the entorhinal cortex of the freely behaving rat. J. Neurosci. *18*, 388–398.

Colgin, L.L., Denninger, T., Fyhn, M., Hafting, T., Bonnevie, T., Jensen, O., Moser, M.B., and Moser, E.I. (2009). Frequency of gamma oscillations routes flow of information in the hippocampus. Nature *462*, 353–357.

Cunningham, M.O., Davies, C.H., Buhl, E.H., Kopell, N., and Whittington, M.A. (2003). Gamma oscillations induced by kainate receptor activation in the entorhinal cortex in vitro. J. Neurosci. *23*, 9761–9769.

Deuchars, J., West, D.C., and Thomson, A.M. (1994). Relationships between morphology and physiology of pyramid-pyramid single axon connections in rat neocortex in vitro. J. Physiol. *478*, 423–435.

Dhillon, A., and Jones, R.S. (2000). Laminar differences in recurrent excitatory transmission in the rat entorhinal cortex in vitro. Neuroscience *99*, 413–422.

Dickson, C.T., Biella, G., and de Curtis, M. (2000). Evidence for spatial modules mediated by temporal synchronization of carbachol-induced gamma rhythm in medial entorhinal cortex. J. Neurosci. *20*, 7846–7854.

Fourcaud-Trocmé, N., Hansel, D., van Vreeswijk, C., and Brunel, N. (2003). How spike generation mechanisms determine the neuronal response to fluctuating inputs. J. Neurosci. *23*, 11628–11640.

Fries, P. (2009). Neuronal gamma-band synchronization as a fundamental process in cortical computation. Annu. Rev. Neurosci. *32*, 209–224.

Fuhs, M.C., and Touretzky, D.S. (2006). A spin glass model of path integration in rat medial entorhinal cortex. J. Neurosci. *26*, 4266–4276.

Fyhn, M., Molden, S., Witter, M.P., Moser, E.I., and Moser, M.B. (2004). Spatial representation in the entorhinal cortex. Science *305*, 1258–1264.

Garden, D.L., Dodson, P.D., O'Donnell, C., White, M.D., and Nolan, M.F. (2008). Tuning of synaptic integration in the medial entorhinal cortex to the organization of grid cell firing fields. Neuron *60*, 875–889.

Goodman, D., and Brette, R. (2008). Brian: a simulator for spiking neural networks in python. Front. Neuroinform. *2*, 5.

Guanella, A., Kiper, D., and Verschure, P. (2007). A model of grid cells based on a twisted torus topology. Int. J. Neural Syst. *17*, 231–240.

Hafting, T., Fyhn, M., Molden, S., Moser, M.B., and Moser, E.I. (2005). Microstructure of a spatial map in the entorhinal cortex. Nature *436*, 801–806.

Hafting, T., Fyhn, M., Bonnevie, T., Moser, M.B., and Moser, E.I. (2008). Hippocampus-independent phase precession in entorhinal grid cells. Nature *453*, 1248–1252.

Huxter, J., Burgess, N., and O'Keefe, J. (2003). Independent rate and temporal coding in hippocampal pyramidal cells. Nature *425*, 828–832.

Klausberger, T., and Somogyi, P. (2008). Neuronal diversity and temporal dynamics: the unity of hippocampal circuit operations. Science *321*, 53–57.

Koenig, J., Linder, A.N., Leutgeb, J.K., and Leutgeb, S. (2011). The spatial periodicity of grid cells is not sustained during reduced theta oscillations. Science *332*, 592–595.

Krupic, J., Burgess, N., and O'Keefe, J. (2012). Neural representations of location composed of spatially periodic bands. Science *337*, 853–857.

Kumar, S.S., Jin, X., Buckmaster, P.S., and Huguenard, J.R. (2007). Recurrent circuits in layer II of medial entorhinal cortex in a model of temporal lobe epilepsy. J. Neurosci. *27*, 1239–1246.

Lisman, J. (2005). The theta/gamma discrete phase code occuring during the hippocampal phase precession may be a more general brain coding scheme. Hippocampus *15*, 913–922.

Mason, A., Nicoll, A., and Stratford, K. (1991). Synaptic transmission between individual pyramidal neurons of the rat visual cortex in vitro. J. Neurosci. *11*, 72–84.

McNaughton, B.L., Barnes, C.A., and O'Keefe, J. (1983). The contributions of position, direction, and velocity to single unit activity in the hippocampus of freely-moving rats. Exp. Brain Res. *52*, 41–49.

McNaughton, B.L., Battaglia, F.P., Jensen, O., Moser, E.I., and Moser, M.B. (2006). Path integration and the neural basis of the 'cognitive map'. Nat. Rev. Neurosci. *7*, 663–678.

Middleton, S., Jalics, J., Kispersky, T., Lebeau, F.E., Roopun, A.K., Kopell, N.J., Whittington, M.A., and Cunningham, M.O. (2008). NMDA receptor-dependent switching between different gamma rhythm-generating microcircuits in entorhinal cortex. Proc. Natl. Acad. Sci. USA *105*, 18572–18577.

Mitchell, S.J., Rawlins, J.N., Steward, O., and Olton, D.S. (1982). Medial septal area lesions disrupt theta rhythm and cholinergic staining in medial entorhinal cortex and produce impaired radial arm maze behavior in rats. J. Neurosci. *2*, 292–302.

Mizuseki, K., Sirota, A., Pastalkova, E., and Buzsáki, G. (2009). Theta oscillations provide temporal windows for local circuit computation in the entorhinal-hippocampal loop. Neuron *64*, 267–280.

Navratilova, Z., Giocomo, L.M., Fellous, J.M., Hasselmo, M.E., and McNaughton, B.L. (2012). Phase precession and variable spatial scaling in a periodic attractor map model of medial entorhinal grid cells with realistic after-spike dynamics. Hippocampus *22*, 772–789.

O'Keefe, J., and Recce, M.L. (1993). Phase relationship between hippocampal place units and the EEG theta rhythm. Hippocampus *3*, 317–330.

Pastoll, H., Ramsden, H.L., and Nolan, M.F. (2012a). Intrinsic electrophysiological properties of entorhinal cortex stellate cells and their contribution to grid cell firing fields. Front Neural Circuits *6*, 17.

Pastoll, H., White, M., and Nolan, M. (2012b). Preparation of parasagittal slices for the investigation of dorsal-ventral organization of the rodent medial entorhinal cortex. J. Vis. Exp. *61*, 3802.

Quilichini, P., Sirota, A., and Buzsáki, G. (2010). Intrinsic circuit organization and theta-gamma oscillation dynamics in the entorhinal cortex of the rat. J. Neurosci. *30*, 11128–11142.

Sargolini, F., Fyhn, M., Hafting, T., McNaughton, B.L., Witter, M.P., Moser, M.B., and Moser, E.I. (2006). Conjunctive representation of position, direction, and velocity in entorhinal cortex. Science *312*, 758–762.

Song, S., Sjöström, P.J., Reigl, M., Nelson, S., and Chklovskii, D.B. (2005). Highly nonrandom features of synaptic connectivity in local cortical circuits. PLoS Biol. *3*, e68.

Tiesinga, P., and Sejnowski, T.J. (2009). Cortical enlightenment: are attentional gamma oscillations driven by ING or PING? Neuron *63*, 727–732.

van Der Linden, S., Panzica, F., and de Curtis, M. (1999). Carbachol induces fast oscillations in the medial but not in the lateral entorhinal cortex of the isolated guinea pig brain. J. Neurophysiol. *82*, 2441–2450.

Welinder, P.E., Burak, Y., and Fiete, I.R. (2008). Grid cells: the position code, neural network models of activity, and the problem of learning. Hippocampus *18*, 1283–1300.

Wilent, W.B., and Nitz, D.A. (2007). Discrete place fields of hippocampal formation interneurons. J. Neurophysiol. *97*, 4152–4161.

Yartsev, M.M., Witter, M.P., and Ulanovsky, N. (2011). Grid cells without theta oscillations in the entorhinal cortex of bats. Nature *479*, 103–107.